# Growing Helical Density Waves in Semiconductor Plasmas*

C. E. HURWITZ AND A. L. MCWHORTER
*Lincoln Laboratory† and Electrical Engineering Department, Massachusetts Institute of Technology, Cambridge, Massachusetts*

(Received 2 December 1963)

An experimental and theoretical investigation is made of growing screw-shaped plasma density waves in a semiconductor bar subjected to parallel electric and magnetic fields. A particularly simple mode is used, requiring only a thermal-equilibrium electron-hole plasma, low-recombination surfaces, and moderate fields. It is shown that in extrinsic material the growth is spatial, corresponding to stable traveling-wave amplification, while for nearly equal densities of positive and negative carriers the wave is absolutely unstable and corresponds to the oscillistor phenomenon. Experimental observations of the waves were made in germanium at and above room temperature for frequencies from 20–400 kc and with electric and magnetic fields from 25–60 V/cm and 0–11 kG, respectively. The growth rates and phase characteristics were found to be in excellent agreement with theory and gain in excess of 35 dB/cm was obtained. At higher temperatures, corresponding to nearly intrinsic material, evidence of instability was found in accordance with the theoretical prediction.

## I. INTRODUCTION

HELICAL plasma density waves were originally proposed by Kadomtsev and Nedospasov[1] to account for an instability that occurs in the positive column of a gas discharge in a longitudinal magnetic field. Subsequently, Glicksman[2] suggested that a slightly generalized form of this theory could explain the oscillistor effect in semiconductors.[3–5] In its simplest form the oscillistor is a semiconductor bar that exhibits terminal voltage and/or current oscillations when an electron-hole plasma is created by injection or light generation and sufficiently large parallel electric and magnetic fields are applied. Further refinements of the theory for semiconductors and experimental confirmation of the helical nature of the oscillistor instability have been provided by several other authors,[6–13] leaving no doubt as to the correctness of Glicksman's basic idea. However, the feature from which the oscillistor takes its name, the terminal voltage-current oscillation, has not been adequately accounted for up to now, nor has it been determined whether the oscillation is caused by an absolute instability or a convective instability with feedback.[14–19]

The present work indicates that the oscillistor instability is an absolute one and that the terminal oscillations can result from nonlinearities alone. The bulk of the paper, however, is devoted to the theoretical and experimental investigation of a completely different aspect of these helical waves, that of traveling-wave amplification. In this study, a preliminary account of which has been given earlier,[20] a mode is utilized that is much simpler than the one considered by previous authors and which involves only the thermal-equilibrium hole-electron plasma. In these other treatments the growth was always assumed to be temporal, representing instability, and the possibility of stable amplification was not considered, perhaps because the high degree to which the growth and propagation constants are influenced by the net difference in hole and electron densities was not fully appreciated. It will be shown that using nothing more than a uniform bar of germanium at room temperature with a low-recombination surface, Ohmic contacts, and moderate applied electric and magnetic fields, controlled amplification of as much as 35 dB/cm can be achieved. In the limit of nearly equal hole and electron densities (intrinsic material or material with a high level of injected carriers) the helical wave becomes absolutely unstable, corresponding to the oscillistor situation mentioned above.

---

* Based on a thesis submitted by C. E. Hurwitz to the Massachusetts Institute of Technology in partial fulfillment of the requirements for the degree of Doctor of Philosophy.

† Operated with support from the U. S. Air Force.

[1] B. B. Kadomtsev and A. V. Nedospasov, J. Nucl. Energy **1**, 230 (1960).

[2] M. Glicksman, Phys. Rev. **124**, 1655 (1961).

[3] I. L. Ivanov and S. M. Ryvkin, Zh. Techn. Fiz. **28**, 774 (1958) [English transl.: Soviet Phys.—Tech. Phys. **3**, 722 (1958)].

[4] J. Bok and R. Veilex, Compt. Rend. **248**, 2300 (1958).

[5] R. D. Larrabee and M. C. Steele, J. Appl. Phys. **31**, 1519 (1960).

[6] F. Okamoto, T. Koike, and S. Tosima, J. Phys. Soc. Japan **17**, 804 (1962).

[7] Y. H. Ichikawa, S. Misawa, and Y. Sasakura, Progr. Theoret. Phys. (Kyoto) **27**, 1277 (1962).

[8] T. Misawa, Japan. J. Appl. Phys. **1**, 67 (1962).

[9] T. Misawa, Japan. J. Appl. Phys. **1**, 131 (1962).

[10] B. Ancker-Johnson, *Proceedings of the International Conference on the Physics of Semiconductors, Exeter 1962* (The Institute of Physics and the Physical Society, London, 1962), p. 141; Bull. Am. Phys. Soc. **7**, 496 (1962).

[11] Ø. Holter, Phys. Rev. **129**, 2548 (1963).

[12] R. D. Larrabee, J. Appl. Phys. **34**, 880 (1963).

[13] T. Misawa and T. Yamada, Japan. J. Appl. Phys. **2**, 19 (1963).

[14] R. Q. Twiss, Proc. Phys. Soc. (London) **B64**, 654 (1951).

[15] P. A. Sturrock, Phys. Rev. **112**, 1488 (1958).

[16] L. D. Landau and E. M. Lifshitz, Fluid Mechanics (Pergamon Press, Ltd., London, 1959), pp. 111–114.

[17] Y. B. Fainberg, V. I. Kurilko, and V. D. Shapiro, Zh. Techn. Fiz. **31**, 633 (1961) [English transl.: Soviet Phys.—Tech. Phys. **6**, 459 (1961)].

[18] R. V. Polovin, Zh. Techn. Fiz. **31**, 1220 (1961) [English transl.: Soviet Phys.—Tech. Phys. **6**, 889 (1962)].

[19] A. Bers and R. Briggs, Research Laboratory of Electronics, MIT, Quarterly Progress Report No. 71, 1963, p. 122 (unpublished).

[20] C. E. Hurwitz and A. L. McWhorter, Phys. Rev. Letters **10**, 20 (1963); Bull. Am. Phys. Soc. **8**, 206 (1963).

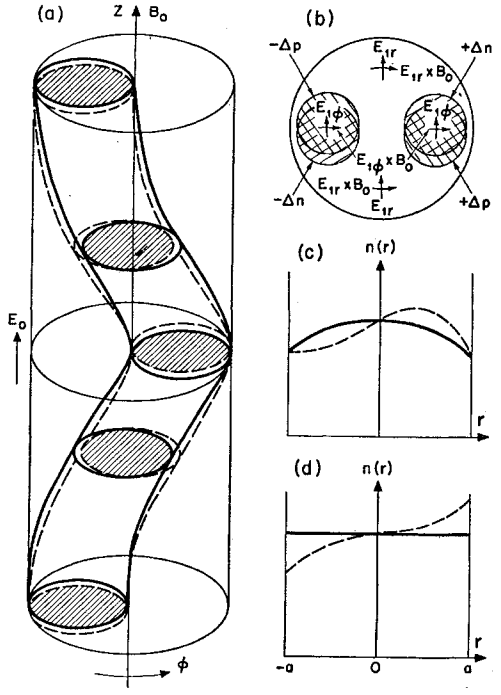


FIG. 1. Right-handed helical perturbation for $|m|=1$. (a) Perturbed-electron distribution indicated by dashed lines and perturbed hole distribution by solid lines. [After Hoh and Lehnert (Ref. 21).] (b) Cross-sectional view showing charge separation and resulting perturbed electric fields $E_1$. Directions of carrier flow due to the combined effect of $E_1$ and $B_0$ are indicated by the vectors $\mathbf{E}_1\times\mathbf{B}_0$. (c) and (d) Carrier density versus radius along a horizontal diameter through the cross section of (b) for the equilibrium-gradient mode and the surface-density mode, respectively. Solid lines correspond to unperturbed distributions and dashed lines to distributions altered by radial and azimuthal flows.

## II. PHYSICAL MODEL

A physical model of the growth mechanism of the helical wave was developed by Hoh and Lehnert[21,22] for the gas-discharge case. We will include an additional part of the mechanism and modify the picture to apply to semiconductors. The argument is begun by assuming a small, quasineutral, screw-shaped perturbation of positive and negative carriers to be superimposed on the steady-state unperturbed distribution. The general form, in cylindrical coordinates, would be $F(r)\exp(i\omega t-ikz-im\phi)$ with $F(r)$ determined by the boundary condition at the wall; however, for the present argument we consider only the lowest mode $m=\pm 1$, as the full mathematical treatment shows that this mode has the lowest threshold for growth. The perturbation is shown schematically in Fig. 1(a) for $m$ and $k$ having opposite signs (a right-handed helix). The longitudinal electric field $E_0$ tends to separate the superimposed positive and negative screws axially, which is equivalent to a rotation of one screw relative to the other, as shown in Fig. 1(a) and in the cross-sectional view of Fig. 1(b). The resulting charge separation creates both an azimuthal and a radial electric field, $E_{1\phi}$ and $E_{1r}$, respectively. The radial field was neglected by Hoh and Lehnert but it is no less important than the azimuthal field in the description of the total growth mechanism. In the linear approximation these fields, together with the longitudinal magnetic field $B_0$, act on the unperturbed distribution to produce a radial and azimuthal flow of particles, indicated in Fig. 1(b) by the vectors $\mathbf{E}_{1\phi}\times\mathbf{B}_0$ and $\mathbf{E}_{1r}\times\mathbf{B}_0$. If the unperturbed distribution has a radial gradient, as it does in a gas discharge or in the usual form of the oscillistor (due to the finite recombination of injected carriers at the walls), this flow is not divergenceless and hence can feed particles from the main distribution into the screw with the proper phase, thus producing a growth of the perturbation. This may be seen more clearly in Fig. 1(c), where the carrier density is plotted as a function of radius along a diameter horizontally through the cross section of Fig. 1(b). For the signs of $E_0$ and $B_0$ chosen, the flow adds carriers to the assumed excess in the region $r>0$ and removes carriers from the assumed deficit in the region $r<0$, thus enhancing the perturbation.

When the influx of particles is sufficiently large to overcome the dissipative effects of diffusion and recombination the helix will grow. It may thus be expected that for a given value of electric field $E_0$ there will be a threshold value of magnetic field $B_{0c}$ above which growth is observed. There should also be an optimum wavelength, for if the wavelength is too long the charge separation and therefore the driving electric fields will be too small, while for a very short wavelength the diffusive effects will take over and dissipate the perturbation. If the sample or plasma column is long enough that end effects are negligible, the wavelength should be independent of the sample length. For the electric and magnetic fields as shown in Fig. 1(a) the screw of opposite sense will clearly be attenuated since the radial and azimuthal flows now reverse directions and tend to destroy the perturbation. In general it may be stated[9] that the helix which can exhibit growth is right- (left-) handed for the electric and magnetic fields parallel (antiparallel).

In a semiconductor a radial gradient of the unperturbed distribution can be produced in thermal equilibrium by proper doping (e.g., by indiffusion or outdiffusion of impurities), eliminating the need for a steady-state injected or optically-generated plasma with all of its inherent complications. Of course, the radial gradients of the holes and electrons in this "equilibrium-gradient mode" will be in opposite directions, producing a partial cancellation in the growth process, but as shown in a calculation of the threshold for this mode in Appendix A there can still be a net buildup of the perturbation.

However, except for this calculation, we will be concerned with an even simpler mode of semiconductor operation requiring no unperturbed radial gradient at

[21] F. C. Hoh and B. Lehnert, Phys. Rev. Letters **7**, 75 (1961).
[22] F. C. Hoh, Phys. Fluids **5**, 22 (1962).

all, merely a sufficiently low surface recombination. In this mode, called here the "surface-density mode," growth occurs because the radial and azimuthal flows can pile up or deplete the carriers at the surface in the proper phase, as illustrated in Fig. 1(d). The role of the dc-electric and magnetic fields in producing the flow is the same as before. Experimentally the surface-density mode is easier to achieve than the equilibrium-gradient mode, and also the mathematical theory for the surface-density mode can be formulated with fewer approximations.

In addition to the growth properties, the motion of the wave can also be ascertained from the physical model. As is well known, a quasineutral density perturbation under the influence of an applied electric field $E_0$ propagates in the direction of minority carrier drift with a velocity $v_d=\mu_a E_0$, with $\mu_a$, the ambipolar drift mobility, being given by

$$\mu_a=[\mu_e\mu_h(n_0-p_0)]/(n_0\mu_e+p_0\mu_h),$$

where $n_0$ and $p_0$ are the equilibrium densities of electrons and holes, and $\mu_e$ and $\mu_h$ are their respective mobilities. Thus, the helix performs a bodily translation with the ambipolar drift velocity $v_d$. In addition, there is a rotation of the helix due to diffusion and conduction of carriers across the magnetic field. (Another mechanism for rotation, due to the radial ambipolar electric field, also exists when the unperturbed carrier distribution has a radial gradient.) The total motion of the helix is composed of these two parts. For extrinsic semiconductors the translation will dominate, while for intrinsic semiconductors the ambipolar mobility is zero and the motion is therefore purely rotational. Discussion of the direction of rotation will be postponed until the next section where the necessary mathematical expressions are derived. It should be noted that because of the nature of a helix both motions when viewed in any cross-sectional plane produce a rotation of the carrier density and field patterns about the axis.[23]

The ambipolar drift of the helix also plays a crucial role in distinguishing instability from stable growth. A detailed discussion is presented in the next section, but to complete the physical picture the basic ideas are outlined here. Three fundamental processes govern the change in amplitude of the perturbation with time at any point in space: the growth mechanism previously described, diffusion, and ambipolar drift down the bar. Above threshold the growth is enough to overcome diffusion, but for a sufficiently large drift velocity the disturbance is swept away, growing as it moves. At any point in space the perturbation remains bounded in time, and the result is simply a spatially growing wave. However, if the ambipolar drift velocity is very small the perturbation may build up faster than it can diffuse and drift away. At a point in space it may then grow temporally, corresponding to an absolute instability. Clearly the first case is pertinent to extrinsic semiconductors, and the latter to semiconductors with nearly equal electron and hole densities and to gaseous plasmas.

It should also be mentioned that Gurevich and Ioffe[24] have proposed a very similar mechanism which can lead to growing density waves in thin semiconductor slabs. In their model a steady-state density gradient and electric fields are set up either by illumination of one surface or by the Hall effect. Then the addition of a wave-like density perturbation creates a perturbed electric field through charge separation in the steady-state electric and magnetic fields. As in the case of the helical wave, this perturbed field acts on the unperturbed distribution to produce a carrier flow in the correct direction to enhance the perturbation. The applied electric and magnetic fields perform different functions in the chain of physical argument, but the fundamental process of coupling an unperturbed density gradient with a perturbed electric field to achieve growth is basically the same as for the helical wave. Experimental observations of instability under conditions similar to those considered by Gurevich and Ioffe have been reported[25,26] and may well be explained in terms of their model.

## III. MATHEMATICAL THEORY

With the preceding physical picture in mind, we now formulate a quantitative mathematical description of the helical wave in the surface-density mode. The equilibrium-gradient mode is considered in Appendix A. Using the equations of motion and continuity for electrons and holes, the dispersion relation governing the growth and propagation of the helical wave will be derived. From this equation will then follow both the threshold conditions and the growth and phase constants for stable growth as well as the threshold for instability.

Consider a cylindrical bar of semiconductor, long in the $z$ direction so that end effects may be neglected. The bar is assumed to be uniform and in thermal equilibrium and therefore to contain a uniform density $n_0$ of electrons and $p_0$ of holes with $n_0-p_0=N_D-N_A$, where $N_D$ and $N_A$ are the densities of ionized donor and acceptor impurities, respectively. Under the assumption that the times and distance of interest are much larger than the mean free times and paths of the free carriers, we may write the following equations to describe the behavior of

[23] The contribution of the drift motion to this rotation was first pointed out by Okamoto *et al.* (Ref. 6).

[24] L. E. Gurevich and I. V. Ioffe, Fiz. Tverd. Tela **4**, 2641, 2964 (1962) [English transl.: Soviet Phys.—Solid State **4**, 1938, 2173 (1963)].

[25] S. Nakashima and Y. Miyai, J. Phys. Soc. Japan **18**, 1219 (1963).

[26] S. Nakashima and Y. Noguchi, Japan. J. Appl. Phys. **2**, 307 (1963).

the carriers under applied electric and magnetic fields:

$$\mathbf{J}_e = nq\mu_e\mathbf{E} + qD_e\nabla n - \mu_e\mathbf{J}_e\times\mathbf{B}, \quad (1)$$

$$\mathbf{J}_h = pq\mu_h\mathbf{E} - qD_h\nabla p + \mu_h\mathbf{J}_h\times\mathbf{B}, \quad (2)$$

$$\partial n/\partial t = (1/q)\nabla\cdot\mathbf{J}_e + \gamma, \quad (3)$$

$$\partial p/\partial t = -(1/q)\nabla\cdot\mathbf{J}_h + \gamma, \quad (4)$$

$$\nabla\cdot\mathbf{E} = -q(n-p)/\epsilon. \quad (5)$$

The subscripts $e$ and $h$ refer to the electrons of density $n$ and holes of density $p$, respectively; $\mu$ is the mobility, $D$ is the diffusion constant, $\gamma$ is the net rate of bulk generation (which in the absence of trapping is the same for both carriers), $\epsilon$ is the dielectric constant of the semiconductor, $q$ is the magnitude of the electronic charge, $J$ is the current density, and $E$ and $B$ are the electric and magnetic fields, respectively.

In order to effect a considerable simplification in the mathematics it will be assumed throughout that the square of the Hall angle for each carrier is small; i.e., that $\mu_{e,h}^2B^2 \ll 1$. Under this assumption and also assuming that the self-magnetic fields are negligible with respect to the applied uniform magnetic field $B_0$, Eqs. (1)–(4) may be combined to yield

$$\partial n/\partial t = n\mu_e\nabla\cdot\mathbf{E} + \mu_e\mathbf{E}\cdot\nabla n + D_e\nabla^2 n + \mu_e^2\mathbf{E}\cdot(\nabla n\times\mathbf{B}_0), \quad (6)$$

and

$$\partial p/\partial t = -p\mu_h\nabla\cdot\mathbf{E} - \mu_h\mathbf{E}\cdot\nabla p + D_h\nabla^2 p + \mu_h^2\mathbf{E}\cdot(\nabla p\times\mathbf{B}_0). \quad (7)$$

The bulk generation term has been omitted as it is a simple matter to reinsert it if desired near the end of the calculation.

Equations (6) and (7) are now linearized for small perturbations about equilibrium by writing

$$n = n_0 + n_1, \quad p = p_0 + p_1, \quad E = E_0 - \nabla\psi_1, \quad (8)$$

where the subscripts 0 and 1 refer to the equilibrium quantities and their perturbations, respectively. Assuming quasineutrality (i.e., $n_1 \approx p_1$, but $\nabla^2\psi_1 \neq 0$), eliminating $\psi_1$ from the linearized equations, and restricting ourselves to the particular case of interest where $E_0$ and $B_0$ are both in the $z$ direction, we have the familiar ambipolar continuity equation for $n_1$:

$$\partial n_1/\partial t = D_a\nabla^2 n_1 - \mu_a E_0(\partial n_1/\partial z), \quad (9)$$

where

$$\mu_a \equiv [\mu_e\mu_h(n_0-p_0)]/(n_0\mu_e + p_0\mu_h)$$

and (10)

$$D_a \equiv (n_0\mu_e D_h + p_0\mu_h D_e)/(n_0\mu_e + p_0\mu_h)$$

are the ambipolar mobility and diffusion constant, respectively.

To obtain the normal modes for the problem, the perturbations $n_1$ and $\psi_1$ are Fourier analyzed in cylindrical coordinates $(r,\phi,z)$ in the form

$$n_1 = N_1(r)\exp(i\omega t - ikz - im\phi),$$
$$\psi_1 = \Psi_1(r)\exp(i\omega t - ikz - im\phi), \quad (11)$$

and (9) is solved for $N_1(r)$, the radial part of $n_1$, with the result

$$N_1(r) = c_1 I_m(\beta r), \quad (12)$$

where $I_m(\beta r)$ is the modified Bessel function of the first kind of order $m$, $c_1$ is an arbitrary constant, and

$$\beta^2 \equiv [(\omega - \mu_a E_0 k)/D_a] + k^2. \quad (13)$$

The potential $\Psi_1(r)$ is obtained from the continuity equations (6) and (7), which after linearization and for $E_0$ and $B_0$ in the $z$ direction may be combined in the form

$$\nabla^2\psi_1 + A\nabla^2 n_1 = 0, \quad (14)$$

where

$$A \equiv -i\frac{E_0 k(\mu_e+\mu_h)}{(n_0\mu_e+p_0\mu_h)(\beta^2-k^2)} + \frac{D_e - D_h}{n_0\mu_e + p_0\mu_h}. \quad (15)$$

Therefore,

$$\psi_1 = An_1 + \text{a solution of Laplace's equation.} \quad (16)$$

The appropriate solution of Laplace's equation is a modified Bessel function $I_m(kr)$, and as a result

$$\Psi_1(r) = Ac_1 I_m(\beta r) + c_2 I_m(kr). \quad (17)$$

To complete the solution, the boundary condition at the surface $r=a$ of the cylinder must be applied. These conditions have the form

$$-(1/q)J_{er}(a) = (1/q)J_{hr}(a) = sn_1(a), \quad (18)$$

where $J_{er}(a)$ and $J_{hr}(a)$ are respectively the radial components of the electron and the hole current at the surface, $s$ is the surface recombination velocity and $n_1(a)$ is the excess carrier density at the surface. From (1) and (2), for $E_0$ and $B_0$ in the $z$ direction and for $\mu_{e,h}^2B_0^2 \ll 1$, we have to first order in the perturbation quantities

$$-\frac{1}{q}J_{er} = n_0\mu_e\left(\frac{\partial\psi_1}{\partial r} - \frac{\mu_e B_0}{r}\frac{\partial\psi_1}{\partial\phi}\right) - D_e\left(\frac{\partial n_1}{\partial r} - \frac{\mu_e B_0}{r}\frac{\partial n_1}{\partial\phi}\right) \quad (19)$$

and

$$\frac{1}{q}J_{hr} = -p_0\mu_h\left(\frac{\partial\psi_1}{\partial r} + \frac{\mu_h B_0}{r}\frac{\partial\psi_1}{\partial\phi}\right) - D_h\left(\frac{\partial n_1}{\partial r} + \frac{\mu_h B_0}{r}\frac{\partial n_1}{\partial\phi}\right). \quad (20)$$

Substituting these expressions into (18) and introducing the solutions (11), (12), and (17) into the resulting equations we obtain two linear, homogeneous equations for the coefficients $c_1$ and $c_2$. The dispersion relation relating the frequency $\omega$ and propagation constant $k$ is obtained by setting the determinant of these equations equal to zero. The result, after inserting the value of $A$ from (15) and performing some algebraic manipulation,

is the following equation:

$$(m\mu_M^2E_0B_0/D_a)[k/(\beta^2-k^2)]$$
$$\times[\beta I_m'(\beta a)I_m(ka)-kI_m(\beta a)I_m'(ka)]$$
$$+a\beta kI_m'(\beta a)I_m'(ka)-im\mu_HB_0\beta I_m'(\beta a)\,I_m(ka)$$
$$+[(sa/D_a)-im\mu_aB_0]kI_m(\beta a)I_m'(ka)$$
$$-im\mu_HB_0(s/D_a)I_m(\beta a)I_m(ka)=0, \quad (21)$$

where $\mu_a$, the ambipolar mobility, is as defined in (10),

$$\mu_H=R_H\sigma_0=(p_0\mu_h^2-n_0\mu_e^2)/(n_0\mu_e+p_0\mu_h) \quad (22)$$

is the mixed conduction Hall mobility, and

$$\mu_M^2=n_0p_0\mu_e\mu_h(\mu_e+\mu_h)^2/(n_0\mu_e+p_0\mu_h)^2 \quad (23)$$

is a quantity with the dimensions of mobility squared which appears also in the theory of transverse magnetoresistance. In obtaining (21) use has been made of the definition (10) of $D_a$ and, consistent with the earlier approximation $\mu_{e,h}^2B_0^2\ll1$, a term in $B_0^2$ has been dropped.

This dispersion relation (21) is rather complex and extremely difficult to treat as it stands. Besides being transcendental, it contains both $\omega$ and $k$ in the arguments of the Bessel functions (through the quantity $\beta$). Fortunately, for much of the region of interest it is a reasonable approximation to expand the Bessel functions in Taylor series to obtain an algebraic equation for $\omega$ and $k$. In the section on experimental results some numerical solutions of (21) will be presented which indicate the range of validity of these expansions. Further, since we are dealing with the surface-density mode, it is expected that surface recombination will have to be small in order to obtain growth. Therefore, we make the approximation that $s\ll D_a/a$ and neglect the terms involving $s$. In addition, it is assumed that bulk recombination is also sufficiently small so that $\tau_b\ll a^2/D_a$, which makes it unnecessary to reinsert the bulk recombination term. In Appendix B the modifications due to recombination are taken into account and it is found that for the experimental situation of interest the correction is negligible.

For simplicity we consider here only the lowest order $|m|=1$ mode as this mode has the lowest threshold for growth. In Appendix C the general $m$ mode is considered. Expanding the Bessel functions, we keep only the first two terms of the Taylor series, which will be valid as long as $\beta^2a^2$ and $k^2a^2\ll20$. Substituting the expansions in (21), neglecting terms in $\beta^2k^2$, and eliminating $\beta^2$ by means of (13) we obtain for the simplified dispersion relation:

$$k^2a^2[3+2i(\mu_e-\mu_h)B_0]+i(a^2/2D_a)$$
$$\times(\omega-\mu_aE_0k)[3-i(3\mu_H+\mu_a)B_0]$$
$$+(\mu_M^2E_0B_0/D_a)ka^2+4[1+i(\mu_e-\mu_h)B_0]. \quad (24)$$

## Threshold Conditions

As discussed in Sec. II, it is expected that for a given electric field there should be a critical magnetic field and a critical frequency at which growth is first observed. At this point, which we shall call the threshold, the frequency $\omega$ and propagation constant $k$ are both real, corresponding to neither growth nor attenuation. Therefore, at threshold the real and imaginary parts of (24) may be separated and $\omega$ eliminated between the resulting equations. Neglecting terms of order $\mu_{e,h}^2B_0^2$ compared with unity the result is

$$3k^2a^2+(\mu_M^2E_0B_0/D_a)ka^2+4=0. \quad (25)$$

It is evident that only the product $E_0B_0$ enters (25). Since we seek the minimum value of the applied fields for which growth is first observed we minimize the $E_0B_0$ product with respect to $k$. In this manner we obtain from (25) the threshold value of $k$, denoted by $k_c$:

$$k_c^2=4/3a^2, \quad (26)$$

and also the threshold value of $E_0B_0$. For ease in comparing theory with experiment, the latter is written as an expression for the threshold magnetic field $B_{0c}$, which is then a function of $E_0$:

$$B_{0c}=-\frac{6k_cD_a}{m\mu_M^2}\frac{1}{E_0}, \quad (27)$$

with $|m|=1$.

The critical frequency $f_c$ is obtained from (24). Since at threshold $E_0\sim B_{0c}^{-1}$ from (27), we must consider two limiting cases in order to remain consistent with the assumption $\mu_{e,h}^2B_0^2\ll1$. For extrinsic material, such that $|(n_0-p_0)/(n_0+p_0)|\gg\mu_{e,h}^2B_0^2$, all terms except the one involving $\mu_a$ are neglected, so that

$$f_c=(1/2\pi)\mu_aE_0k_c. \quad (28)$$

For intrinsic or nearly intrinsic material, where $|(n_0-p_0)/(n_0+p_0)|\ll\mu_{e,h}^2B_0^2$, only the terms in $\mu_{e,h}B_0$ are retained, with the result

$$f_c=-(20mD_a/9\pi a^2)(\mu_e-\mu_h)B_{0c}. \quad (29)$$

Equation (28) corresponds to the translation of the helix at the ambipolar drift velocity ($\mu_aE_0$), while (29) corresponds to the rotation of the helix due to diffusion and conduction across the magnetic field. In the intermediate case $|(n_0-p_0)/(n_0+p_0)|\approx\mu_{e,h}^2B_0^2$, the total motion is composed of both translation and rotation; however, a correct expression for $f_c$ cannot be obtained in the approximation $\mu_{e,h}^2B_{0c}^2\ll1$.

From (26) it is evident that just the magnitude of $k_c$ is determined. This is simply a consequence of the fact that for a wave of the form $\exp(i\omega t-ikz-im\phi)$ only the relative signs of $k$, $m$, and $\omega$ are significant. We will choose the signs of $k_c$ and $m$ to make $f_c>0$ in (28) or (29) and to satisfy (27). The resulting signs of $\omega$, $k$, and $m$ for various directions of $E_0$ and $B_0$ and for different types of material are listed in Table I. We have assumed $\mu_e>\mu_h$. The sense and motion of the helix may be deduced immediately from this table.

In agreement with the predictions of the physical

TABLE I. Relative signs of $\omega$, $k$, and $m$ for helical wave of proper sense to permit growth.

| Directions of $E_0$ and $B_0$ | $n$-type material | $p$-type material | Intrinsic material |
|---|---|---|---|
| $E_0>0$ $B_0>0$ | $\omega>0$ $k>0$ $m<0$ | $\omega>0$ $k<0$ $m>0$ | $\omega>0$ $k>0$ $m<0$ |
| $E_0>0$ $B_0<0$ | $\omega>0$ $k>0$ $m>0$ | $\omega>0$ $k<0$ $m<0$ | $\omega>0$ $k>0$ $m>0$ |
| $E_0<0$ $B_0<0$ | $\omega>0$ $k<0$ $m>0$ | $\omega>0$ $k>0$ $m<0$ | $\omega>0$ $k<0$ $m>0$ |
| $E_0<0$ $B_0>0$ | $\omega>0$ $k<0$ $m<0$ | $\omega>0$ $k>0$ $m>0$ | $\omega>0$ $k<0$ $m<0$ |

model, the helix that can exhibit growth is right- (left-) handed for $B_0$ parallel (antiparallel) to $E_0$, irrespective of the type of material. In each case the screw of opposite sense has no threshold and is always attenuated, as will be seen in a subsequent calculation of the growth constant. In any cross-sectional plane, the direction in which the helix appears to revolve about its axis is independent of the direction of $E_0$ and reverses sign with a reversal of $B_0$. Further, for a given $E_0$ and $B_0$ this direction of apparent revolution is the same for $n$-type and intrinsic material and is in the opposite direction for $p$-type material.

## Growth and Phase Constants

Having established that a threshold for growing helical waves does indeed exist and having calculated the critical fields, wave number, and frequency, we now examine in detail the functional behavior of the propagation constant of the waves both above and below threshold. In particular we will consider sufficiently extrinsic material that the waves exhibit only stable spatial growth. The question of instability will be taken up in detail later and it will be seen just how extrinsic the material must be to assure stable growth.

We seek solutions of the dispersion relation in the form of traveling waves, excited at a specific frequency and varying spatially. Therefore, $\omega$ is considered to be a real variable and $k$ is allowed to become complex, i.e., $k=k_r+ik_i$, where $k_r$ is the phase constant and $k_i$ the growth constant. The wave will then travel with phase velocity $v_{ph}=\omega/k_r$ and will vary in amplitude as $\exp(k_i z)$. Equation (24) is now solved directly for $k$, and for material sufficiently extrinsic that

$$\mu_a E_0 \gg D_a/a, \tag{30a}$$

$$|(n_0-p_0)/(n_0+p_0)| \gg \mu_{e,k}^2 B_0^2, \tag{30b}$$

and

$$(\mu_a E_0)^2 \gg \omega D_a, \tag{30c}$$

the square root in the quadratic formula can be expanded in a Taylor series. In performing the expansion we retain real terms to first order and imaginary terms to second order. Further, we choose the root corresponding to the negative square root; the other choice leads to $k_i \approx \mu_a E_0/2D_a$ which by (30a) is much greater than unity and is thus not self-consistent with the earlier Bessel function expansion. Actually the full transcendental dispersion relation leads to an infinite number of other roots, which presumably correspond to strongly damped modes. For the correct root we have

$$k \approx (\omega/\mu_a E_0) - i(8D_a/3a^2\mu_a E_0)[1+\tfrac{3}{4}(\omega a/\mu_a E_0)^2 + (\omega a^2 \mu_M^2 B_0/4\mu_a D_a)]. \tag{31}$$

A considerable simplification of this result may be achieved through the use of the previously derived expressions (27) and (28) for the threshold frequency and magnetic field. The propagation constant $k=k_r+ik_i$ is then

$$k \approx \frac{\omega}{\mu_a E_0} + i\frac{8D_a}{3a^2\mu_a}\frac{1}{E_0}\left[2\frac{fB_0}{f_c B_{0c}} - \left(\frac{f}{f_c}\right)^2 - 1\right]. \tag{32}$$

Equation (32) corresponds to the helical wave of proper sense to permit growth, as given by Table I. The propagation constant for the wave of opposite sense is obtained by simply reversing the sign of the term $(2fB_0/f_c B_{0c})$.

Since $k_r \gg k_i$, we have from (32)

$$v_{\text{phase}} = v_{\text{group}} = \mu_a E_0, \tag{33}$$

confirming our earlier assertions that for extrinsic material the wave translates with the ambipolar drift velocity.

We see further that the wave will grow spatially ($k_i>0$ for waves traveling in the direction of increasing $z$ and $k_i<0$ for those propagating in the opposite direction) when

$$2B_0/B_{0c} > (f/f_c)+(f_c/f) \tag{34}$$

and the wave of opposite sense is always attenuated.

Actually the existence of a value of $k_i$ of the correct sign for growth is not sufficient to prove that the solution corresponds to a growing wave; it might also be an evanescent wave, such as in a waveguide beyond cutoff. However, the experimental results confirm the fact that (32) is a true growing wave solution, and we need not investigate this point further.

## Instability

In the earlier discussion of the physical model for the helical wave it was reasoned that for sufficiently small ambipolar drift velocity a disturbance could grow temporally rather than spatially, resulting in instability as opposed to stable growth. We shall now derive this result mathematically by developing a quantitative stability criterion for the surface density mode of operation.

Stability criteria and the important distinction between convective growth and absolute instability in systems with growing wave behavior have been discussed by several authors.[14–19] The problem is essentially one of determining the response of the system to a spatially and temporally bounded, but otherwise arbitrary, excitation. If the response (which may be any physical quantity of interest) is bounded as $t \to \infty$ then the system is stable, and it is absolutely unstable otherwise. Assuming that only one dimension need be considered and

that end boundaries are sufficiently far removed so that reflected waves are of no significance, it can be shown that for the purposes of determining the stability it is sufficient to investigate the response $\phi(z,t)$ to a $\delta$-function excitation in space and time:

$$\phi(z,t)=\int_{C_L} e^{i\omega t}d\omega\int_{C_F}\frac{e^{-ikz}}{D(k,\omega)}dk, \tag{35}$$

where $D(k,\omega)=0$ is the dispersion relation for the system under consideration. The Laplace contour $C_L$ runs in the lower half of the $\omega$ plane, below all singularities of the integrand, i.e., $-\infty-i\nu<\omega<\infty-i\nu$, where $\nu$ is a large positive number. For convenience we have set $s=i\omega$ in the conventional Laplace formulation. The Fourier contour $C_F$ is as usual along the real $k$ axis. For positive $t$ the $\omega$-integration contour is closed by a semicircle at infinity in the upper half-plane, and the $k$ contour is closed in the upper or lower half-plane when the region of interest is for $z<0$ or $z>0$, respectively.

In general the integrals in (35) will be difficult and several authors[14–19] have proposed techniques for obtaining the stability information without explicitly evaluating these integrals. However, for the simplified helical-wave dispersion relation (24) for the surface-density mode, the integrations in (35) can be performed directly to investigate the behavior of $\phi(z,t)$ for large $t$. From the physical model presented in Sec. II it is expected that instability will be possible only for nearly equal densities of positive and negative carriers, so for simplicity we set $n_0=p_0$ in most terms of (24). However, we do not set $\mu_a=0$, and thereby retain the very important terms involving the quantity $(n_0-p_0)$. This turns out to be equivalent to neglecting terms of the order of $(n_0-p_0)/(n_0+p_0)$ with respect to unity, but not with respect to quantities of order $\mu_{e,h}B_0$, which are much less than unity. This level of approximation will be maintained throughout the calculation. In several places we shall neglect to set $n_0=p_0$ purely to preserve the form of particular terms and to aid in their identification later; however, it is to be understood that the following calculations are correct only for $n_0\approx p_0$.

Equation (24), after rationalization of the leading term, may then be written in the form (assuming $\mu_{e,h}{}^2B_0{}^2\ll 1$ as usual):

$$D(k,\omega)=(k-k_0)^2-\alpha(\omega-\omega_0)=0, \tag{36}$$

where

$$k_0\equiv -m\mu_e\mu_hE_0B_0/6D_a+i[\mu_a/4D_a+\mu_e\mu_h(\mu_e-\mu_h)B_0{}^2/9D_a]E_0, \tag{37a}$$

$$\omega_0\equiv -(m\mu_e\mu_hE_0{}^2B_0/6)[\mu_a/D_a-5\mu_e\mu_h(\mu_e-\mu_h)B_0{}^2/3D_a]+\imath[8D_a/3a^2+(\mu_aE_0)^2/8D_a-\mu_M{}^4E_0{}^2B_0{}^2/18D_a]. \tag{37b}$$

$$\alpha\equiv[m(\mu_e-\mu_h)B_0-3i]/6D_a. \tag{37c}$$

Focusing our attention on the Fourier integral of (35) in the $k$ plane, we see that only contributions to the integral will be at values of $k=k(\omega)$ such that $D(k,\omega)=0$. As the notation implies, these values of $k$ depend parametrically on $\omega$, where $\omega$ assumes all values on the Laplace contour $C_L$. Referring to (36) it is clear that there will be two lines of zeros of $D(k,\omega)$ in the $k$ plane, corresponding to the two solutions

$$k_\pm(\omega)=k_0\pm[\alpha(\omega-\omega_0)]^{1/2}, \tag{38}$$

where

$$\omega=\omega(C_L). \tag{39}$$

Since $C_L$ is below all singularities of the integrand in the $\omega$ plane, we may immediately conclude that the two lines of zeros do not cross the real $k$ axis and that all of the zeros are simple. Further, using (37c) and (38) in (36) and recalling that $\nu$ may be an arbitrary large positive number, it is clear that $k_+(\omega)$ corresponds to the line of zeros in the upper half $k$ plane, and $k_-(\omega)$ to that in the lower half-plane.

Since the zeros of $D(k,\omega)$ are simple, the poles of the integrand at $k=k_\pm(\omega)$ are also simple and the integral over $k$ can be evaluated using the theory of residues. For $z>0$ the contour is closed in the lower half-plane enclosing the line of zeros corresponding to $k=k_-(\omega)$. The solution for $z<0$ proceeds analogously and will not be detailed. We may thus write for the response:

$$\phi(z,t)=\exp(-ik_0z)\int_{C_L}\frac{\exp\{i\omega t+i[\alpha(\omega-\omega_0)]^{1/2}\}}{[\alpha(\omega-\omega_0)]^{1/2}}d\omega. \tag{40}$$

The integral in (40) may be evaluated directly from a table of Laplace transforms,[27] with the result

$$\phi(z,t)=\frac{1}{(\alpha t)^{1/2}}\exp\left(i\omega_0t-i\frac{a}{4t}-ik_0z\right). \tag{41}$$

Writing $\omega_0=\omega_{0r}+i\omega_{0i}$, we immediately conclude that the system will be stable or absolutely unstable depending on whether $\omega_{0i}$ is positive or negative.

It therefore follows from (37b) that a long semiconductor bar with a low-recombination surface and with applied parallel electric and magnetic fields $E_0$ and $B_0$ will be stable ($\omega_{0i}>0$) when

$$(\mu_aE_0)^2+(8D_a/a\sqrt{3})^2\geq(\tfrac{2}{3}\mu_M{}^2E_0B_0)^2 \tag{42}$$

and will exhibit absolute instability when the inequality is reversed.

We may now make a plausible identification of the terms of (42). The quantity $\mu_aE_0$ is simply the ambipolar drift velocity. The term $(8D_a/a\sqrt{3})$ is in the form of a diffusion velocity and is a measure of the effective velocity at which carriers diffuse out of the helix. To aid in the identification of the last term we note that the earlier results on the threshold for growth may be put in a form similar to (42). From (26) and (27) we may write that growth will obtain when

$$(\tfrac{2}{3}\mu_M{}^2E_0B_0)^2>(8D_a/a\sqrt{3})^2. \tag{43}$$

[27] See, for example, R. V. Churchill, *Operational Mathematics* (McGraw-Hill Book Company, Inc., New York, 1958), p. 328.

The right-hand term is again the square of the effective diffusion velocity. Since it is diffusion which must be overcome to obtain growth, we may conclude that the left-hand term is the square of the effective velocity at which carriers are driven into the helix by the combined action of $E_0$ and $B_0$, corresponding to the growth mechanism.

With these identifications in mind we may write the three quantities in (42) as $v_{\text{drift}}^2$, $v_{\text{diff}}^2$, and $v_{\text{growth}}^2$, respectively. From (42) and (43) it may then be stated that the helical wave will exhibit stable traveling-wave amplification when

$$v_{\text{drift}}^2+v_{\text{diff}}^2>v_{\text{growth}}^2>v_{\text{diff}}^2, \tag{44}$$

and will be unstable when the first inequality is reversed.

Although the above discussion is based on a plausible and not rigorously justified identification of terms in (42) and (43), we see that (44) leads us to essentially the same conclusions reached by physical reasoning. That is, when the flow of particles due to the growth mechanism is sufficiently strong to overcome diffusion, a disturbance will grow but will be swept away from its point of origin and spatial growth will result. Further, when the flow is sufficient to overcome both diffusion and drift, the disturbance will build up temporally at its point of origin, resulting in instability. It is not clear, however, why the above expressions involve the squares of the various velocities. Although these velocities are actually complex vectors, and some components will therefore be in either or both time and space quadrature, no explanation of the form of (44) has yet been obtained on this basis.

Several further interesting conclusions may be drawn from Eqs. (42)–(44). For $n_0 \neq p_0$ the threshold for growth is lower than that for instability, and consequently as $B_0$ is increased for fixed $E_0$ the system passes successively from attenuated waves to stable growing waves to instability. For $n_0$ exactly equal to $p_0$, however, there is no region of stable gain and above threshold the system is immediately unstable. The instability threshold value of $E_0$ decreases monotonically with increasing $B_0$, but there is a minimum value of $B_0$ given by

$$B_{0,\min}=3\mu_a/2\mu_M^2 \tag{45}$$

below which there can be no instability regardless of the value of $E_0$. The instability threshold value of $B_0$ also decreases monotonically with $E_0$ and although (42) predicts no corresponding minimum $E_0$ for instability, there presumably is such a minimum due to saturation of the growth term when $\mu_{e,h}B_0 \gg 1$. The terms which lead to this saturation have, of course, been neglected throughout the calculations.

Finally, we may calculate the frequency and wave number at which instability is first predicted, i.e., when $\omega_{0i}=0$ and (42) becomes an equality. These quantities are just $\omega_{0r}$ and $k_{0r}$, respectively, and are given by (37a) and (37b), where $E_0$ and $B_0$ are the instability threshold values and are related by (42) with the inequality sign replaced by an equal sign.

## IV. EXPERIMENTAL PROCEDURE

In order to provide quantitative verification of the theory presented in the preceding section, a long, uniform cylindrical semiconductor sample was required with accurately known carrier densities and mobilities and with bulk and surface recombination sufficiently low that $\tau_b \gg a^2/D_a$ and $s \ll D_a/a$. Further, it was necessary that the longitudinal electric field, pulsed to avoid heating, be applied by means of truly Ohmic contacts in order not to alter the uniform equilibrium carrier distribution. Finally, a means of exciting and detecting the helical wave without altering the number of minority carriers was required.

The samples were fabricated from high-quality, uncompensated $n$-type germanium with a room-temperature resistivity of about 30 ohm-cm and a bulk lifetime of 1400 $\mu$sec. Accurate values for the carrier densities at each temperature of interest (290–360°K) were computed from the value of $n-p=N_D-N_A=3.16\times10^{13}$, obtained by Hall measurements at 77°K, plus the reported value[28] of the $np$ product. In order to ensure that the net donor density was given correctly by the usual expression $N_D-N_A=-(R_Hq)^{-1}$, where $R_H$ is the Hall coefficient, the measurements were made with a magnetic field of 20 kG oriented in a ⟨001⟩ crystallographic direction.[29] Further, the Hall sample had a length-to-width-ratio of 6 to prevent shorting of the Hall field by the end contacts.[30] The uncertainty in the resulting value of $N_D-N_A$ is estimated to be $\pm3\%$.

Carrier-drift mobilities were obtained by scaling the reported[31] lattice mobilities at 300°K according to the experimentally obtained[32] power law appropriate to each carrier for lattice scattering; i.e., $\mu_e=(3900)(T/300)^{-1.66}$ and $\mu_h=(1900)(T/300)^{-2.33}$. This computation was felt to be fully valid in view of the fact that in high-quality uncompensated germanium, lattice scattering is completely dominant in this temperature range.[31,32] Further, the measured resistivities at each temperature (using voltage probes and electric fields of about 0.05 V/cm to avoid complications due to contacts) agreed well within experimental error with the values calculated from the above densities and mobilities.

Samples of both square and circular cross section were used. The samples were first lapped and then etched to final size to remove all damaged surface layers. Dimensions after etching were approximately 25 mm long $\times$ 1 mm diam for the cylindrical samples and $25\times1\times1$ mm for those of square cross section. To comply with the requirement of the theory, the samples should be much longer than the attenuation length of

[28] F. J. Morin and J. P. Maita, Phys. Rev. **94**, 1525 (1954).
[29] W. M. Bullis and W. E. Krag, Phys. Rev. **101**, 580 (1955).
[30] C. Dunlap, *An Introduction to Semiconductors* (John Wiley & Sons, Inc., New York, 1957), p. 186.
[31] M. B. Prince, Phys. Rev. **92**, 681 (1953).
[32] F. J. Morin, Phys. Rev. **92**, 62 (1954).

any reverse wave so that the presence of the ends cannot be communicated to a significant portion of the bar. Since it is not known theoretically if a reverse wave does exist and if so what its properties are, the sample length was arbitrarily made approximately ten times the threshold wavelength [see Eq. (26)]. Experimentally, no significant effects due to end boundaries were observed.

The etching procedure was quite complex and has been described in detail elsewhere.[33] Using this procedure, which was concluded by protecting the surfaces with silicone oil, it was possible to achieve and maintain surface recombination velocities which were regularly less than 50 cm/sec and often as low as 20 cm/sec. These values of $s$ were computed[34] from the lifetime of injected carriers, measured by decay of photoconductivity for each sample, and the similarly measured bulk lifetime of the original crystal.

The relatively high-resistivity material and strong electric fields (20–60 V/cm) precluded the use of the usual methods for making Ohmic contacts. Metallic soldered, plated, or alloyed contacts always gave $p^+n$ or $n^+n$ junctions which interfered with the flow of carriers. Depending on the direction of current flow a $p^+n$ contact injected or extracted holes while an $n^+n$ contact excluded or accumulated them. Sandblasting the surfaces near the contact to recombine an excess or make up a deficit of minority carriers failed because the electric field swept the carriers through any practical recombination-generation region much faster than they could diffuse to or from the surface.

The problem was solved by use of the arrangement shown in Fig. 2. Only one end of the bar is labeled but the other end is identical. The $p^+$ contact carries only the hole current and the parallel $n^+$ contacts carry only the electron current. The series resistors are much larger than the contact resistances. Thus, by adjusting the variable resistor in series with the $p^+$ contact, the relative electron and hole currents can be set to precisely the values required to maintain the thermal-equilibrium carrier distribution. The large resistors make the setting independent of the electric field, but of course the variable resistor has to be readjusted for each temperature of operation. With respect to fabrication, excellent contacts were formed by alloying In+1/2% Ga and Sn+5% Sb spheres to the sample followed by electrolytic etching.[33]

Excitation and detection of the waves were accomplished by means of pairs of small $n^+$ probes attached to the surface of the sample (see Fig. 2). These $n^+n$ junctions conduct majority carriers (electrons) freely but are impervious to the flow of minority carriers (holes).[35]

Thus when a pair of probes (such as aa′) is driven

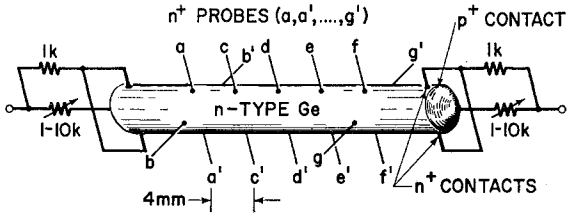


FIG. 2. Sketch of cylindrical sample, showing Ohmic end contacts and $n^+$ probes.

with an ac signal source, the electric field produced causes the holes to move back and forth in synchronism, perturbing the carrier distribution and initiating the wave. Actually, the linearly polarized excitation just described excites both the $m=\pm 1$ modes, but as discussed in the last section, one mode will always decay while the other can grow. By using two sets of probes (aa′ and bb′, for example) which are 90° apart around the circumference and driving them with two signals 90° out of time phase, one or the other of the circularly polarized modes may be excited preferentially.

The use of the $n^+$ probes in detecting the helical wave makes use of the fact that the electron quasi-Fermi level (QFL) is constant through the $n^+n$ junctions. The open-circuit voltage between two probes then gives the difference between the electron QFL's just beneath the surface at the two points. However, for small signals the perturbed electron QFL is linearly related[36] to the perturbations in the density and potential, i.e.,

$$\phi_{e1}\approx\psi_1-(kT/q)(n_1/n_0).$$

Therefore, all information pertaining to the amplitude and phase characteristics of the waves may be obtained by measuring $\phi_{e1}$ with $n^+$ probes. Of course, it is also necessary that the contacts be impervious to the flow of holes in order to prevent their generation or recombination in the junctions.

These probes were fabricated by bonding 0.002-in. Sb-doped Au wires to the sample with pulses of current.[37] To assure that the two probes of a set (c and c′, for example) were aligned on the same cross-sectional plane of the sample, an electrical null technique was used to locate them.[33] All probes were checked for proper operation by using them to measure known changes in the electron QFL produced by illuminating the sample with penetrating light.[33] This test was also correlated with the current-voltage characteristics of the probes.

A diagram of the arrangement for the above-described excitation and detection of the waves is shown in Fig. 3. The phase shifter and probe driver provided signals 90° out of phase from low-impedance sources. The input impedance of the detecting and measuring circuits was

[33] C. E. Hurwitz, MIT Lincoln Laboratory Technical Report No. 320, 1963 (unpublished).
[34] W. Shockley, *Electrons and Holes in Semiconductors* (D. Van Nostrand Company, Inc., New York, 1950), pp. 318–325.
[35] A. K. Jonscher, *Principles of Semiconductor Device Operation* (G. Bell and Sons, London, 1960), pp. 142–144.
[36] W. Shockley, *Electrons and Holes in Semiconductors* (D. Van Nostrand Company, Inc., New York, 1950), p. 308.
[37] M. C. Waltz, in *Transistor Technology*, edited by H. E. Bridges, J. H. Scaff, and J. N. Shive (D. Van Nostrand Company, Inc., Princeton, 1958), Vol. I, pp. 375–380.

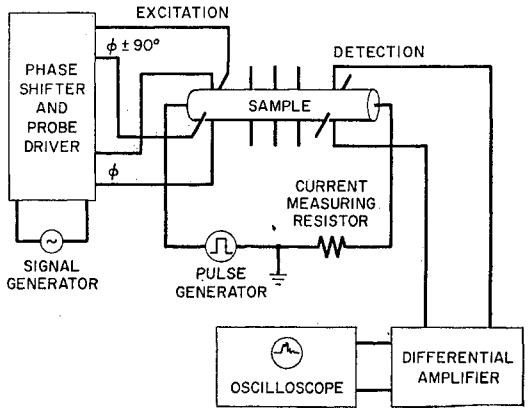


FIG. 3. Experimental arrangement for exciting and detecting helical waves. The differential amplifier may be connected to any desired set of probes.

sufficiently high to provide "open circuit" conditions up to frequencies in excess of 500 kc.

The completed sample, mounted in a jig, was attached to a holder which permitted rotation of the sample in a vertical plane for accurate alignment parallel to the magnetic field. This arrangement was mounted between the poles of an electromagnet which was rotatable in the horizontal plane to complete the alignment of sample and field. The sample and lower part of the holder were immersed in a bath of silicone oil which was maintained at a constant, controllable temperature. A thermocouple mounted on the jig next to the sample read the actual temperature. In this manner the temperature could be set and held to within $\pm 0.1°C$ of the desired value.

## V. EXPERIMENTAL RESULTS AND COMPARISON WITH THEORY

The basic experiment consisted of applying parallel dc-magnetic and pulsed-electric fields to the sample, exciting the wave with a signal source at an appropriate set of probes, and then observing the excitation in magnitude and phase as it traveled down the bar.

Many samples of both square and circular cross section were fabricated and examined experimentally. All exhibited spatially growing waves whose properties agreed qualitatively with the predictions of the physical model and the mathematical theory. However, due to the involved fabrication procedure and the finite-failure rate at each step (a full set of properly operating $n^+$ probes was particularly difficult to achieve), only two samples, one square and one circular, were judged to fully meet the requirements discussed in the previous section and therefore to be suitable for accurate quantitative measurements. As will become evident in the following discussion, the agreement between experiment and theory is sufficiently good that although results for only two samples are reported, the theory can be considered completely verified in the region of stable growth.

The final dimensions of these two samples were 1.16 mm diam by 25.4 mm long for the cylindrical sample and $1.02 \times 1.02 \times 25.4$ mm for the one of square cross section.

The temperature of operation proved to be a particularly valuable parameter to vary as it provided a test of the functional dependence of the wave properties on the equilibrium carrier densities without the need for many samples of varying resistivities. In fact, by raising the temperature it was possible to pass from the extrinsic region in which stable spatial growth is observed to nearly intrinsic material where some of the considerations of instability and the oscillistor are of interest.

The extremely low yield of good samples precluded the use of sample geometry as another variable. The dependence on sample radius seems well enough confirmed by the general quantitative agreement of all measurements, but the question of how long is a "long" sample and the length dependence of the threshold in samples comparable in size to a wavelength would still be of interest. Except where otherwise stated, the data to be presented refer to the sample of circular cross section, for in this case there is no ambiguity as to the value of radius to be used in the theoretical expressions.

### Helical Waveshape

The helical nature of the wave was confirmed by exciting the sample at probes aa′ and observing the relative phase of the resulting signals at probes ff′ and gg′. (See Fig. 2. The electric field is positive from left to right.) The resulting waveforms are shown in Fig. 4, and we see that for $B_0$ parallel to $E_0$ the signal at gg′ led that at ff′ by 90° and lagged by 90° when $B_0$ was reversed. The traces shown are for threshold, but the same phase relationship was found for all fields and frequencies. Adding to this result the fact that the phase and group velocities are in the direction of the electric field (see next section) it is clear that we do indeed have a helical wave, traveling in the direction of ambipolar drift, which as predicted is right- (left-) handed for $B_0$ parallel (antiparallel) to $E_0$.

Further, when a circularly polarized excitation was provided by driving probes aa′ and bb′ with signals 90° out of time phase, only the polarization direction cor-

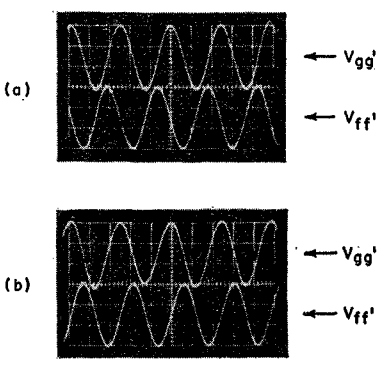


FIG. 4. Oscilloscope traces showing 90° phase difference between signals at probes gg′ and ff′. Set (a) corresponds to $B_0$ parallel to $E_0$ and (b) to $B_0$ antiparallel to $E_0$. Vertical scale: 5 mV/div. Horizontal scale: 10 μsec/div.

responding to the predicted screw sense produced a growing wave. The opposite excitation produced only a strongly attenuated wave. That is, for excitation in the sense a → b′ → a′ → b the wave grew (for fields above threshold) for $B_0$ parallel to $E_0$ and always decayed when $B_0$ was reversed. For excitation in the sense a → b → a′ → b′ the converse was true. These results are in full agreement with the predictions of the physical model, Eq. (32) and Table I.

### Phase Constant—Phase and Group Velocity

For a wave of the form $\exp[i\omega t-i(k_r+ik_i)z\pm i\phi]$ the phase difference $\Delta\Phi$ between two points differing in $z$ by $\Delta z$ at the same instant of time and same value of $\phi$ is simply

$$\Delta\Phi=-k_r\Delta z.$$

Thus the measurement of the relative phase of the signal at two sets of probes, such as dd′ and ff′, gives directly the phase constant $k_r$. In Fig. 5 we plot $-\Delta\Phi$, the amount by which the phase at ff′ lags that at dd′, and the resulting value of $k_r$, as a function of $f/E_0$ for several temperatures and electric fields. The probe spacing $\Delta z$ in this case was 0.8 cm. Since the probes were several wavelengths apart there was always an uncertainty of $2n\pi$ in the absolute phase difference as related to that measured. However, for the extrinsic case we assume that we have a simple wave so that the extrapolated value of $\Delta\Phi$ is zero for $\omega=0$. Therefore, to each set of experimental points (at a given temperature) we have added an appropriate multiple of $2\pi$. For each set of points the required translation was always $2n\pi$ and $n$ was just that integer required to make $k_r=2/a\sqrt{3}$ at threshold, in agreement with (26).

The measured values of $\Delta\Phi$ and therefore $k_r$ were, within experimental error, independent of magnetic field over the range 0–11 kG for all temperatures except 67°C and above, but in the latter range exhibited a very slight dependence at the lowest frequency and highest

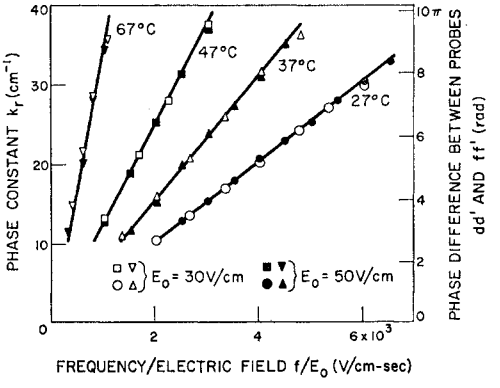


FIG. 5. Phase constant $k_r$ (left-hand scale), computed from measured phase difference between probes dd′ and ff′ (right-hand scale), versus $f/E_0$, for several temperatures and electric fields. Points are experimental; curves are theoretical, calculated from Eq. (32).

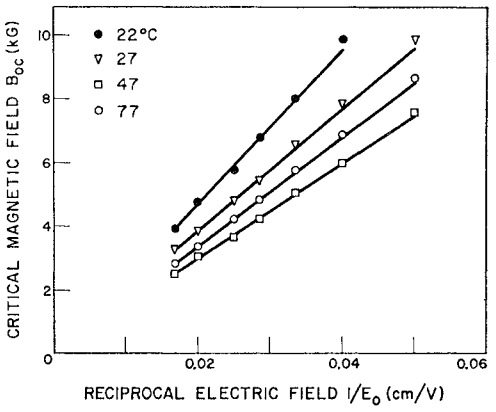


FIG. 6. Critical magnetic field $B_{0c}$ versus $1/E_0$ for several temperatures. Points are experimental; curves are theoretical, calculated from Eq. (27).

magnetic fields. The theoretical curves were calculated from (32) and agreement is excellent. The slopes of the straight lines are just $\mu_a/2\pi$ and therefore, as predicted, $v_{\text{phase}}=v_{\text{group}}=\mu_aE_0$, the ambipolar drift velocity. Values of $k_r$ obtained by numerical computation from the full dispersion relation (21) were insignificantly different from those given by (32).

### Threshold Conditions

The threshold, by definition, is the point at which the $z$ variation of the wave first changes from attenuation to growth. At this point $k_i=0$ and the signal at each set of detecting probes must have the same magnitude. For a fixed electric field, the threshold frequency $f_c$ and magnetic field $B_{0c}$ were obtained by exciting the wave at probes aa′ and bb′ and then slowly raising the magnetic field while sweeping the frequency back and forth. The field and frequency at which the signals at probes dd′, and ee′, and ff′ first became equal were then the threshold values. For properly operating probes these signals became equal simultaneously. The signal at probes cc′ was usually slightly larger, presumably due to higher modes which had not decayed sufficiently that near to the excitation.

In Figs. 6 and 7 we have plotted the measured values of $f_c$ and $B_{0c}$ as a function of the applied electric field $E_0$ for various temperatures. The theoretical curves were calculated from (27) and (28). Agreement is again very good. The small deviations from theory of the values of $f_c$ at the higher temperatures, lowest electric fields, and highest magnetic fields are presumably due to the beginning influence of the rotational contribution to the frequency. At high magnetic fields, $B_{0c}$ also begins to deviate from theory due to breakdown of the assumption $\mu_{e,h}{}^2B_0{}^2\ll1$. Note, however, that at moderate fields the theoretical and experimental values of $B_{0c}$ agree very well at all temperatures. This is to be expected since no assumptions concerning the relative carrier densities were made in the theoretical calculation of

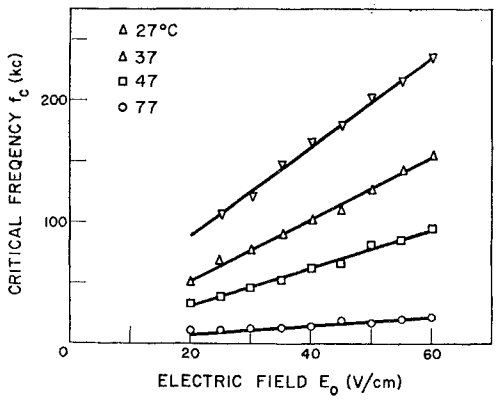


FIG. 7. Critical frequency $f_c$ versus $E_0$ for several temperatures. Points are experimental; curves are theoretical, calculated from Eq. (28).

$B_{0c}$. As the temperature increases and $(n_0-p_0)\rightarrow 0$, $f_c$ decreases rapidly, but $B_{0c}$ quickly approaches a limiting value which is independent of the magnitude of $n_0$ and $p_0$, as may be seen from Eq. (27). However, when the mobilities are decreasing functions of temperature, as is the case here, $B_{0c}$ reaches a minimum and then increases slightly with temperature. Thus, as we see in Fig. 6, the values of $B_{0c}$ at 77°C are somewhat higher than at 47°C.[38]

## Growth Constant

The exponential variation of the wave amplitude in the $z$ direction was confirmed by measurement of the relative signal magnitudes at probes dd′, ee′, and ff′, with excitation provided at aa′ and/or bb′. More precisely, as long as the excitation was sufficiently small that the signal at any set of probes was less than 500 mV peak-to-peak, the wave varied longitudinally as $\exp(k_i z)$ where $k_i$ is the growth constant. When the signal rose above this level, saturation effects began to set in and the linearized theory no longer applied. More will be said about nonlinear effects in the next section; in the present discussion we limit ourselves to the small-signal linear region.

Figures 8 and 9 show the theoretical and experimental variation of the growth constant $k_i$ as a function of $B_0$ for various temperatures and values of $E_0$. In all cases the frequency was fixed at the threshold value $f_c$ pertinent to the specific temperature and electric field. The dashed curves are calculated from (32); the full curves are the results of the exact (in the limit $\mu_{e,h}^2B_0^2\ll 1$) numerical solution of the full dispersion equation, (21). The approximate solution is clearly accurate only in the neighborhood of threshold ($k_i=0$), and deviates both above and below threshold where the Bessel function expansions are no longer correct. The experimental results agree very well with the theoretical curves except at high magnetic fields where the assumption $\mu_{e,h}^2B_0^2\ll 1$ becomes a poor approximation. Numerical solutions were not obtained for the higher temperatures, but the excellent quantitative agreement between experiment and theory at lower temperatures indicates that the agreement should be equally good. Intermediate values of electric field, omitted from Fig. 9 for clarity, also gave quantitatively correct results.

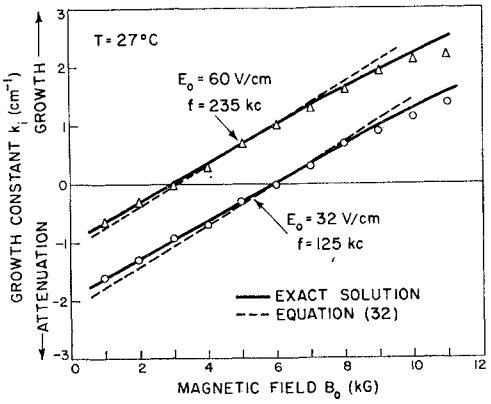


FIG. 8. Growth constant $k_i$ versus $B_0$ for two values of $E_0$, at $T=27$°C and $f=f_c$. Points are experimental; solid curves are exact theoretical solutions for $\mu_{e,h}^2B_0^2\ll 1$, and dashed curves are calculated from Eq. (32).

[38] Since all measurements were made with small signals, no hysteresis effects such as described by B. Ancker-Johnson [Appl. Phys. Letters 3, 104 (1963)] were observed.

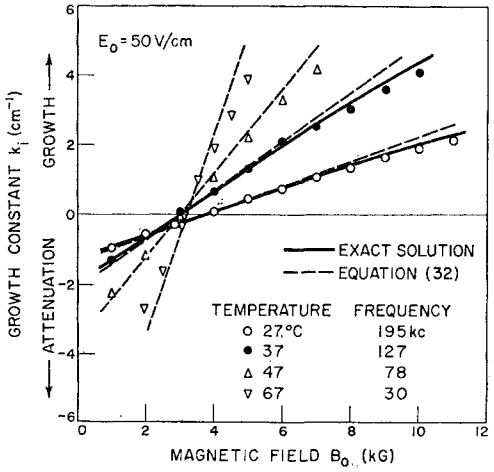


FIG. 9. Growth constant $k_i$ versus $B_0$ for several temperatures at $E_0=50$ V/cm and $f=f_c$. Points are experimental; solid curves are exact theoretical solutions for $\mu_{e,h}^2B_0^2\ll 1$, and dashed curves are calculated from Eq. (32).

Note the rapid increase of growth constant with temperature in Fig. 8. The highest measurable value of $k_i$ was about 4 cm$^{-1}$, corresponding to a gain of approximately 35 dB/cm. For growth rates above this value the sample began to amplify appreciably its internal noise to values comparable with the maximum signal amplitudes obtainable under linear operation.

The frequency dependence of the growth constant is detailed in Figs. 10 and 11, where for $E_0=50$ V/cm the theoretically predicted and measured values of $k_i$ have been plotted as a function of frequency at $T=27°C$ and $T=37°C$ for three values of magnetic field: $B_0<B_{0c}$, $B_0\approx B_{0c}$, and $B_0>B_{0c}$. Again the dashed curves are calculated from (32) and the full curves are the solutions obtained by numerical computation. The inadequacy of the simplified theory, except in the neighborhood of threshold, is strikingly evident. Equally apparent is the extremely good agreement between the experimental points and the exact theory.

In Figs. 12 and 13 similar measurements of $k_i$ as a function of $B_0$ and $f$ for the sample of square cross section are presented. An effective radius $a=0.053$ cm was chosen in plotting the theoretical curves from (32) in order to give the best fit to the experimental data. This choice is very nearly the radius of a cylinder with the same cross-sectional area as the sample. No numerical solutions were obtained for this case but, in light of the results for the circular sample, the behavior at frequencies and fields above threshold would presumably be in agreement with the exact solution. The gross disagreement at low frequencies, which is more than could be accounted for by the exact theory, is only an apparent one. It is due to the fact that linearly polarized (two-probe) excitation was used rather than the circularly polarized (four-probe) excitation employed for all measurements on the cylindrical sample. Examination of (32) shows that for $f<f_c$ and $B_0<B_{0c}$ the right- and left-handed helices have comparable attenuation rates. Since both are excited approximately equally, the measured value of $k_i$ will be some combination of the two. This identical discrepancy was later noted on the cylindrical sample, but was eliminated by using four-probe excitation. Because the square samples were by then of little interest, no attempt was made to redo the earlier measurements.

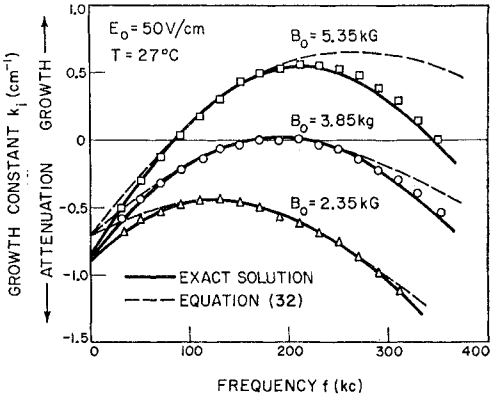


FIG. 10. Growth constant $k_i$ versus $f$ for $B_0<B_{0c}$, $B_0\approx B_{0c}$, and $B_0>B_{0c}$, at $T=27°C$ and $E_0=50$ V/cm. Points are experimental; solid curves are exact theoretical solutions for $\mu_{e,h}{}^2B_0{}^2\ll 1$, and dashed curves are calculated from Eq. (32).

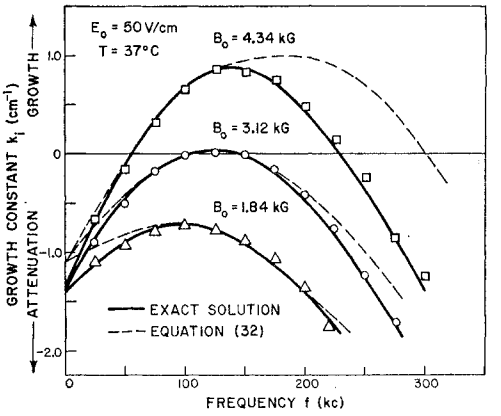


FIG. 11. Growth constant $k_i$ versus $f$ for $B_0<B_{0c}$, $B_0\approx B_{0c}$ and $B_0>B_{0c}$, at $T=37°C$ and $E_0=50$ V/cm. Points are experimental: solid curves are exact theoretical solutions for $\mu_{e,h}{}^2B_0{}^2\ll 1$, and dashed curves are calculated from Eq. (32).

An effort to measure directly the functional behavior of $k_i$ for the helix of screw-sense opposite to the one exhibiting growth was made by simply reversing the rotation direction of the four-probe excitation, while maintaining the fields in the same direction. However, due to the fact that four points cannot give a perfect $\exp(i\phi)$ distribution, a sufficient amount of the growing wave was excited to completely obscure the measurements.

Along this same line an attempt was made to excite the next higher $|m|=2$ mode by connecting a and a′ together and b and b′ together, and then driving the resulting two terminals with the signal generator. Such an arrangement should preferentially excite the $|m|=2$ mode. However, again due to the imperfect excitation, enough of the $|m|=1$ mode was excited to drive the sample into strong nonlinear behavior and saturation before the higher $|m|=2$ mode threshold could be reached.

Finally, it should be mentioned here that the growth constant was found to be an extremely sensitive function of the angle between $B_0$ and $E_0$. Figure 14 illustrates this behavior. The value of $k_i$ falls off so rapidly that at an angle greater than $\pm 3°$ the strong attenuation made measurements impossible. The reason for such a striking sensitivity to a very small transverse component of magnetic field is not known. In terms of the physi-

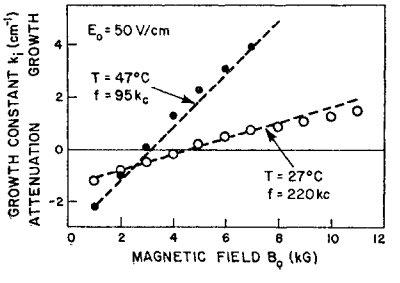


FIG. 12. Growth constant $k_i$ versus $B_0$ for square sample. Points are experimental; curves are theoretical, calculated from Eq. (32) with $a=0.053$ cm.

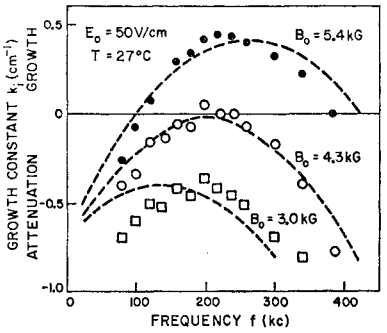


FIG. 13. Growth constant $k_i$ versus $f$ for $B_0<B_{0c}$, $B_0\approx B_{0c}$, and $B_0>B_{0c}$, for square sample. Points are experimental; curves are theoretical, calculated from Eq. (32) with $a=0.053$ cm.

cal model it would seem that the only effect of such a field is to exert a weak transverse force on the carriers, slightly altering their distribution and setting up a small Hall field. Mathematically, the introduction of a transverse component of $B_0$ complicates the problem considerably by destroying the azimuthal symmetry. It might be possible to effect some simplification by introducing the transverse component of field as a perturbation. However, such a calculation has not yet been attempted and the effect remains unexplained.

### Nonlinear Effects and Current Oscillations

As stated earlier, when signals at the probes reached approximately 500 mV peak-to-peak, saturation began to set in, indicating the onset of nonlinear behavior. The probes farthest down the bar (in the direction of $E_0$) saturated first as expected, since the amplified signal is largest there. Further increase of the signal level by raising of the excitation or growth rate successively saturated the level at earlier probes, with the signal reaching a limiting value of about 1.5 V peak-to-peak at all probes. At temperatures of 47°C and above, the gain for large enough magnetic fields could be made sufficient to saturate at least the last probes of the sample on amplified internal noise. The spectral characteristics of this noise were quite unusual and will be the subject of further discussion in connection with current oscillations.

Two important effects were noted in conjunction with the onset of strong saturation, namely a marked increase in the dc sample resistance and appearance of oscillations in the terminal sample current. In Fig. 15 the measured dc resistance of the sample is plotted as a function of increasing magnetic field (and hence increasing growth rate). The point at which the resistance begins to increase over its equilibrium value coincides with nearly full saturation at the farthest set of probes (ff'). Current oscillations, shown in the inset of Fig. 15 begin to come into evidence at the same point.

The sample resistance change is a graphic manifestation of the onset of nonlinear behavior. The perturbed carrier density $n_1$ has now become comparable with the equilibrium densities $n_0$ and $p_0$, and the carriers are strongly bunched into the traveling helix. Although the total number of carriers in the sample has not changed, this bunching has produced a net increase in the resistance. The expected order of magnitude of this resistance change may easily be calculated. When strongly bunched, the carriers will be concentrated near the surface of the sample in a helix with pitch $2\pi/k$ and an effective radius approximately equal to the sample radius $a$. Most of the current will flow between the terminals in this helical path. Both the increased path length of the current and the reduced component of the electric field in the direction of current flow then act to increase the total sample resistance over the equilibrium value. It is a simple matter to show geometrically that the path length is increased by a factor of approximately $(1+k^2a^2)^{1/2}$, and that the component of electric field along the helix is also smaller than the applied fied by the same factor. Thus, with the onset of strong bunching the sample resistance may be expected to increase until it is about a factor of $(1+k^2a^2)$ larger than the unperturbed value. From (26) $k^2a^2\approx 4/3$, so the resistance should approach a value about 2.3 times larger than that for no bunching. The measured values shown in Fig. 15 are in qualitative agreement with this estimate.

On the basis of the linear theory no terminal VI oscillations are predicted. Since all time-varying quantities vary as $\exp[i\omega t-ikz-im\phi]$, $m\neq 0$, the density integrated over a cross section is independent of time and hence there can be no oscillation of the total resistance. Glicksman's assertion that standing waves, set up by reflections at the contacts, can give rise to terminal oscillations[2] is clearly incorrect since the density still varies sinusoidally with $\phi$ and $t$ and the integrated density again vanishes. One must therefore invoke nonlinearities or nonuniformities as the basis of the observed oscillation. Misawa[8] has proposed that mixing in of the $m=0$ mode due to deviations from circular symmetry, such as nonuniformities or transverse components of magnetic field, could account for the behavior, and this possibility cannot be ruled out. In fact Okamoto *et al.*[6] have observed that certain oscillistor samples show current oscillations only in the presence of a small transverse component of magnetic field. However, the above experimental observations that oscillations are present in extremely uniform cylindrical samples with strictly longitudinal fields, and that the onset of current oscillation is always associated directly with the onset of nonlinear behavior, provide

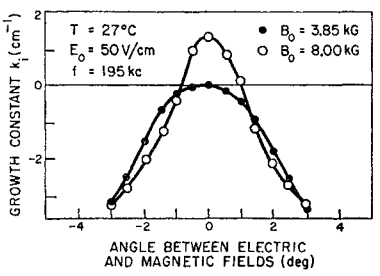


FIG. 14. Growth constant $k_i$ versus angle between $E_0$ and $B_0$.

quite conclusive evidence that large-signal nonlinearity is in itself sufficient to account for terminal oscillations.

The fact that current oscillations were observed in the region of *stable* amplification, requiring only that the gain and excitation be sufficiently large to reach saturation, shows further that instability is not required to obtain such oscillations. In this region the oscillations were essentially sinusoidal at the frequency of excitation, until very strong saturation occurred and some higher harmonic content became apparent. At temperatures below 67°C when the gain was raised sufficiently high to saturate the sample on its own noise, the resultant small current oscillations exhibited a similarly noisy frequency spectrum. However, at 67°C and above, further increase in the magnetic field resulted in a rapid narrowing of the frequency spectrum of both the signals at the probes and the current oscillations, until the frequency was nearly monochromatic and roughly equal to the threshold frequency. One might conceive of a situation in which the strong excursion into nonlinearity might produce a substantial narrowing of the bandwidth for amplification; however, it seems more satisfying to picture the cause as the onset of an instability and the consequent buildup of oscillation at a specific frequency. Indeed just such an instability was predicted from the theory for nearly intrinsic material (i.e., at high temperatures).

Unfortunately, as discussed earlier in connection with the instability theory, a region of stable growth precedes the onset of instability in extrinsic material. The resulting amplification of noise in anything but very nearly or absolutely intrinsic material drives the sample into saturation before instability is attained, so that the linear theory is no longer valid. Such was the case in all of our measurements, even at the highest temperature (87°C). We may, however, make the following qualitative observation. For the 30 ohm-cm germanium used in the measurements, and for $E_0=60$ V/cm and $B_0=11$ kG, the maximum values available with the present arrangement, Eq. (42) predicts that instability will be attainable for temperatures above 60°C. We note also that the rapid narrowing of the frequency spectrum of the amplified noise with increasing fields was observed experimentally only at temperatures above about 67°C. These two facts lead one to the plausible conclusion that this spectral narrowing is the result of the onset of instability and the resulting buildup of oscillations in a narrow band of frequencies; however, further quantitative verification of the theory would certainly be desirable.

Just how close to intrinsic the material must be to reach the instability threshold before nonlinearity occurs may be seen by returning to Eq. (37a) and solving for the growth constant $k_{0i}$ at the point of instability. Neglecting the term $\mu_e\mu_h B_0^2$ which will almost always be negligible, the result is

$$k_{oi}\approx(\mu_a E_0/4D_a)=(qE_0/4kT)[(n_0-p_0)/(n_0+p_0)].$$

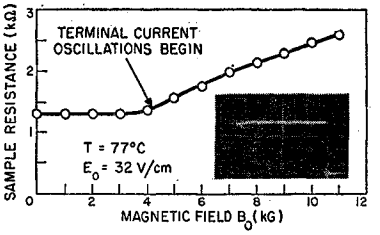


FIG. 15. Average sample resistance versus $B_0$. Inset is oscilloscope trace of terminal current oscillations which begin at the point indicated. Vertical scale: 10 mA/div. Horizontal scale: 200 μsec/div.

Experimentally it was observed that saturation began to set in when $k_i\approx 4$ cm$^{-1}$, and in order to keep $\mu_{e,h}B_0\ll 1$ so that the theory correctly applies, the minimum value of $E_0$ for instability is about 25 V/cm. Therefore we need to have

$$(q/kT)\,|\,(n_0-p_0)/(n_0+p_0)\,|<0.64\text{ V},$$

which for 30 ohm-cm germanium requires $T>100$°C. An easier method would be to start with much purer material. For $N_D-N_A<10^{12}$ cm$^{-3}$ the threshold could be reached while still in the linear region at room temperature.

## The Oscillistor

The above prediction and probable observation of absolute instability in a semiconductor bar, with nearly equal densities of electrons and holes and subjected to sufficiently large parallel and magnetic fields, leads naturally to a discussion of the oscillistor, for it is under precisely these conditions that the effect is observed.[3–5] It was shown experimentally that large signal nonlinearity could give rise to terminal VI oscillations and, of course, the instability can provide the mechanism for the rapid buildup of large signal behavior in the form of a strongly bunched helix of carriers.

Unfortunately the oscillistor effect as it is usually observed and reported in the literature presents such a complicated experimental situation that quantitative comparison with theory is prevented. The attainment of nearly equal carrier densities by double injection into a relatively pure bar of semiconducting (long *p-i-n* structure) leads not only to radial gradients of the carrier distribution but also to substantial longitudinal variations in the steady-state densities and electric field.[39] Such variations are not taken into account by the theory and to do so would hopelessly complicate the mathematics. Further, oscillistor samples are usually made with relatively low surface recombination, and as a result growth is probably due both to the steady-state density gradient and to some piling up of carriers at the surface.

Notwithstanding these complications, the essential features of the instability mechanism remain the same, and one would predict the occurrence of an absolute helical instability under the conditions pertinent to the

[39] M. A. Lampert and A. Rose, Phys. Rev. **121**, 26 (1961).

oscillistor effect. This result coupled with experimental confirmation of the helical nature of the effect,[6,12,13] provides conclusive verification of Glicksman's proposal of a helical instability as the basis of the phenomenon.

Finally, it should be pointed out that for the gaseous plasma the unperturbed densities of electrons and ions are always equal and there is no ambipolar drift of the helical perturbation. There will therefore be no region of stable growth and, as assumed by Kadomtsev and Nedospasov[1] and Hoh and Lehnert,[21,22] only helical instability is possible.

## VI. CONCLUSION

It is evident from the excellent agreement between experiment and theory that the treatment of Sec. III provides an accurate description of the properties of helical waves in the approximation $\mu^2B^2\ll1$. Further, all observations, except the unexpectedly strong dependence of the growth rate on the angle between the electric and magnetic fields, are consistent with the physical model presented in Sec. II.

Although the work was devoted almost entirely to the surface-density mode of operation, it is clear that the general arguments and results may be carried over to more complicated situations, such as the equilibrium-gradient mode or the case of an injected plasma. In addition, although germanium was the only material studied, other semiconductors and perhaps semimetals should exhibit growing helical waves for wide ranges of fields and frequencies, and in fact, oscillistor behavior has been observed in silicon and indium antimonide.[5,10] Unfortunately, in most materials surface and bulk recombination will produce such strong damping of the waves that growth may be difficult to achieve.

## ACKNOWLEDGMENTS

We wish to express our appreciation to A. Bers for many fruitful discussions regarding the analysis of gain and instability. We are also grateful to D. K. Hartman of the General Electric Company for supplying several germanium crystals, A. J. Strauss for help with material evaluation, J. H. R. Ward for valuable technical assistance, and Mrs. Nancy Rawson for performing the numerical computations.

## APPENDIX A: THRESHOLD CONDITIONS FOR EQUILIBRIUM GRADIENT MODE

We again consider a cylindrical sample of radius $a$, long in the $z$ direction, but now assume that the equilibrium carrier densities $n_0$ and $p_0$ are graded in the radial direction. These gradients could be produced, for example, by the outdiffusion of impurities (consider donors to be specific) in which case $n_0$ and $p_0$ would be of the form[40]

$$\begin{aligned} n_0(r)&=n_0J_0(\alpha r),\\ p_0(r)&=n_i^2/n_0(r)=p_0/J_0(\alpha r),\end{aligned} \tag{A.1}$$

where $n_i$ is the intrinsic density. For simplicity we consider the case of weak gradients ($\alpha^2a^2<2$); $n_0$ and $p_0$ may then be written as

$$\begin{aligned} n_0(r)&\approx n_0(1-\alpha^2r^2/4)\\ p_0(r)&\approx p_0(1+\alpha^2r^2/4).\end{aligned} \tag{A.2}$$

We further assume that the surface recombination velocity $s$ is large ($s=\infty$), in order to avoid considering an admixture of the equilibrium-gradient and surface-density modes. As usual it is assumed that the bulk lifetime $\tau_b\gg a^2/D_a$ and that the squares of the Hall angles $\mu_{e,h}^2B_0^2\ll1$.

In equilibrium the continuity equations (6) and (7) become, denoting equilibrium values by the subscript 0,

$$n_0(r)\mu_e\nabla\cdot\mathbf{E}_0+\mu_e\mathbf{E}_0\cdot\nabla n_0(r)+D_e\nabla^2n_0(r)+\mu_e^2\mathbf{E}_0\cdot[\nabla n_0(r)\times\mathbf{B}_0]=0, \tag{A.3}$$

$$p_0(r)\mu_h\nabla\cdot\mathbf{E}_0+\mu_h\mathbf{E}_0\cdot\nabla p_0(r)-D_h\nabla^2p_0(r)-\mu_h^2\mathbf{E}_0\cdot[\nabla p_0(r)\times\mathbf{B}_0]=0. \tag{A.4}$$

The magnetic field $B_0$ as before is in the $z$ direction, whereas the electric field $E_0$, in addition to the applied $z$ component $E_{0z}$, now has a radial ambipolar component $E_{0r}$ due to the density gradients. With equilibrium densities as given in (A.2), Eqs. (A.3) and (A.4) may be readily solved for $E_{0r}$, with the result (assuming $T_e=T_h=T$)

$$E_{0r}\approx(\alpha^2kT/2q)r. \tag{A.5}$$

Following the solution for the surface-density mode, the continuity equations are linearized about equilibrium and quasineutrality is assumed. We then have

$$\frac{\partial n_1}{\partial t}=-\mu_en_0(r)\nabla^2\psi_1+\mu_en_1\frac{1}{r}\frac{\partial}{\partial r}(rE_{0r})+\mu_e\left(E_{0r}\frac{\partial n_1}{\partial r}+E_{0z}\frac{\partial n_1}{\partial z}\right)-\mu_e\frac{\partial n_0(r)}{\partial r}\frac{\partial\psi_1}{\partial r}+D_e\nabla^2n_1+\mu_e^2B_0E_{0r}\frac{1}{r}\frac{\partial n_1}{\partial\phi}+\mu_e^2B_0\frac{1}{r}\frac{\partial\psi_1}{\partial\phi}\frac{\partial n_0(r)}{\partial r}=0, \tag{A.6}$$

and

$$\frac{\partial n_1}{\partial t}=\mu_hp_0(r)\nabla^2\psi_1-\mu_hn_1\frac{1}{r}\frac{\partial}{\partial r}(rE_{0r})-\mu_h\left(E_{0r}\frac{\partial n_1}{\partial r}+E_{0z}\frac{\partial n_1}{\partial z}\right)+\mu_h\frac{\partial p_0(r)}{\partial r}\frac{\partial\psi_1}{\partial r}+D_h\nabla^2n_1+\mu_h^2B_0E_{0r}\frac{1}{r}\frac{\partial n_1}{\partial\phi}+\mu_h^2B_0\frac{1}{r}\frac{\partial\psi_1}{\partial\phi}\frac{\partial p_0(r)}{\partial r}=0. \tag{A.7}$$

[40] The problem is analogous to that of heat flow from a cylindrical rod. See H. S. Carslaw and J. C. Jaeger, *Conduction of Heat in Solids* (Oxford University Press, London, 1959), Ch. VII.

Due to the presence of terms arising from the equilibrium gradients, the equation for $n_1$ may not be decoupled as in the surface-mode solution (9). The coupled equations (A.6) and (A.7) are difficult to treat so, following the Kadomtsev and Nedospasov[1] treatment of the very similar gas-plasma case, we solve the problem only approximately in the following manner. The perturbations are Fourier analyzed as in Eq. (11) and only the lowest $|m|=1$ mode is considered. It is now assumed that $N_1(r)$ and $\Psi_1(r)$ have the approximate form

$$N_1(r)=c_1J_1(\beta_1 r),\qquad \Psi_1(r)=c_2J_1(\beta_1 r), \tag{A.8}$$

where $\beta_1 a$ is the first zero of $J_1$, equal to 3.83, and the $c$'s are constants. Note that $n_1(a)=0$, as required by the assumption $s=\infty$. Equations (A.2), (A.5), and (A.8) are substituted into (A.6) and (A.7) and the resulting equations are averaged over $r$ by multiplying them by $rJ_1(\beta_1 r)$ and integrating with respect to $r$.[41]

We thus obtain the following two algebraic equations for $c_1$ and $c_2$:

$$c_1\{2D_e(k^2+\beta_1^2)-\alpha^2(kT/q)(1+R)+i[2(\omega+\mu_eE_{0z}k)+\alpha^2(kT/q)\mu_e^2B_0]\}+c_2n_0\mu_e\{2(k^2+\beta_1^2)(Q-1)+\alpha^2(1-R)-i\mu_eB_0\alpha^2\}=0, \tag{A.9}$$

and

$$c_1\{2D_h(k^2+\beta_1^2)+\alpha^2(kT/q)(1+R)+i[2(\omega-\mu_hE_{0z}k)+\alpha^2(kT/q)\mu_h^2B_0\}+c_2p_0\mu_h\{2(k^2+\beta_1^2)(Q+1)+\alpha^2(1-R)+i\mu_hB_0\alpha^2\}=0, \tag{A.10}$$

where

$$R\equiv\beta_1\left[\int_0^a rJ_0(\beta_1 r)J_1(\beta_1 r)dr\right]\times\left[\int_0^a rJ_1^2(\beta_1 r)dr\right]^{-1}, \tag{A.11}$$

$$Q\equiv(\alpha^2/4)\left[\int_0^a r^3J^2(\beta_1 r)dr\right]\left[\int_0^a rJ_1^2(\beta_1 r)dr\right]^{-1}. \tag{A.12}$$

The integrals (A.11) and (A.12) are readily evaluated,[42] with the result $R=0$ and $Q=\alpha^2/12\beta_1^2$.

Equations (A.9) and (A.10) are a pair of linear homogenous equations in $c_1$ and $c_2$. The dispersion relation is obtained by setting the determinant of the equations equal to zero. Under the assumptions $\alpha^2\ll\beta_1^2$ and $\mu_{e,h}^2B_0^2\ll1$, we then have, after some straightforward algebra,

$$2D_a(n_0\mu_e+p_0\mu_h)(\beta_1^2+k^2)^2+\alpha^2E_{0z}B_0k\mu_e\mu_h(n_0\mu_e-p_0\mu_h)-\alpha^2\omega B_0(n_0\mu_e^2+p_0\mu_h^2)+i\alpha^2B_0\mu_e\mu_h(kT/q)(\beta_1^2+k^2)\times(n_0\mu_h+p_0\mu_e)+i\alpha^2B_0(\beta_1^2+k^2)(n_0\mu_e^2D_h+p_0\mu_h^2D_e)+i2(\beta_1^2+k^2)(n_0\mu_e+p_0\mu_h)(\omega-\mu_aE_{0z}k)=0, \tag{A.13}$$

where we have employed the definitions (10) of $\mu_a$ and $D_a$.

At threshold $\omega$ and $k$ are real and (A.13) may be separated into real and imaginary parts. Elimination of $\omega$ from the resulting two equations yields

$$(\beta_1^2+k^2)^2+\frac{\alpha^2E_{0z}B_0k}{2D_a}\frac{n_0p_0\mu_e\mu_h(\mu_e^2-\mu_h^2)}{(n_0\mu_e+p_0\mu_h)^2}=0. \tag{A.14}$$

Minimizing the product $E_{0z}B_0$ with respect to $k$ we obtain the threshold conditions:

$$k_c^2=\beta_1^2/3=4.89/a^2, \tag{A.15}$$

and

$$B_{0c}=-\frac{32\beta_1^2k_c}{3m\alpha^2}\frac{D_a(n_0\mu_e+p_0\mu_h)^2}{n_0p_0\mu_e\mu_h(\mu_e^2-\mu_h^2)}\frac{1}{E_0}. \tag{A.16}$$

The result, as expected, is very similar to that for the surface-density mode. The fact that $B_{0c}$ appears to become infinite when $\mu_e=\mu_h$ is a consequence of the fact that the equilibrium gradients of $n_0$ and $p_0$ are in opposite directions, producing a partial cancellation of the growth mechanism. In the simple approximation (A.2) used here these gradients are exactly equal and opposite, so that the cancellation appears to be complete when $\mu_e=\mu_h$. In an exact solution this cancellation would be substantial but not complete.

The threshold frequency is obtained from (A.13) where, as discussed in the derivation of (28) and (29) for the surface-density mode, we take care to remain consistent with the assumption $\mu_{e,h}^2B_0^2\ll1$. We then have for $|(n_0-p_0)/(n_0+p_0)|\gg\mu_{e,h}^2B_0^2$,

$$f_c=(1/2\pi)\mu_aE_{0z}k_c \tag{A.17}$$

which, as before, corresponds to the translation of the helix with the ambipolar drift velocity in extrinsic material.

For intrinsic material, $|(n_0-p_0)/(n_0+p_0)|\ll\mu_{e,h}^2B_0^2$,

$$f_c=-\frac{\alpha^2B_{0c}}{2\pi}\left[\frac{kT}{q}\frac{\mu_e\mu_h(n_0\mu_h+p_0\mu_e)}{n_0\mu_e+p_0\mu_h}+\frac{n_0\mu_e^2D_h+p_0\mu_h^2D_e}{n_0\mu_e+p_0\mu_h}\right]. \tag{A.18}$$

The first term is the rotation due to the built-in ambipolar field $E_{0r}$ and the second term arises from the diffusion and drift of carriers across the magnetic field. Equation (A.19) may be simplified considerably by using the Einstein relation $D_{e,h}=(kT_{e,h}/q)\mu_{e,h}$, assuming $T_e=T_h=T$, and by setting $n_0=p_0$, since (A.19) applies to the nearly intrinsic case. Then

$$f_c=-\frac{m\alpha^2}{2\pi}\frac{kT}{q}\mu_e\mu_hB_{0c}. \tag{A.19}$$

[41] See Refs. 1 and 22 for discussion of the validity of this approximate method.

[42] G. N. Watson, *A Treatise on the Theory of Bessel Functions* (Cambridge University Press, London, 1958), 2nd ed., pp. 132–138.

## APPENDIX B: EFFECT OF SMALL SURFACE AND BULK RECOMBINATION

Equation (9) with the inclusion of the bulk term is

$$\frac{\partial n_1}{\partial t}=D_a\nabla^2 n_1-\mu_a E_0\frac{\partial n_1}{\partial z}-\frac{n_1}{\tau_b}, \tag{B.1}$$

where $\gamma$ has been replaced by $(n-n_0)/\tau_b=n_1/\tau_b$. Recombination has been assumed to take place without trapping so that a single bulk lifetime $\tau_b$ may be used for both carriers. Such a treatment is fully satisfactory for germanium at and above room temperatures. In the Fourier analysis (11), $n\sim e^{i\omega t}$ so that (B.1) can be written in the form

$$(i\omega+1/\tau_b)n_1=D_a\nabla^2 n_1-\mu_a E_0(\partial n_1/\partial z). \tag{B.2}$$

Bulk recombination may therefore be included simply by replacing $\omega$ by $(\omega-i/\tau_b)$ in (24).

To include surface recombination we proceed from (21) exactly as in the derivation of Eq. (25), but now retain the terms involving $s$. As a result for small bulk and surface recombination, (25) is replaced by

$$3k^2a^2+(\mu_M{}^2E_0B_0ka^2/D_a)(1-sa/D_a)+4(1+sa/3D_a)+3a^2/2D_a\tau_b=0, \tag{B.3}$$

where second-order small terms involving $(sa/D_a)^2$ and $(sa/D_a)(a^2/D_a\tau_b)$ and $\mu_{e,h}{}^2B_0{}^2$ have been dropped. Proceeding exactly as in the derivation of (26) and (27) we have finally at threshold:

$$k_c{}^2=\frac{4}{3a^2}\left(1+\frac{sa}{3D_a}+\frac{3a^2}{8D_a\tau_b}\right), \tag{B.4}$$

$$B_{0c}=-\frac{6k_cD_a}{m\mu_M{}^2}\left(1+\frac{sa}{3D_a}\right)\frac{1}{E_0}, \tag{B.5}$$

and

$$f_c=(1/2\pi)\mu_aE_0k_c, \qquad \left|\frac{n_0-p_0}{n_0+p_0}\right|\gg\mu_{e,h}B_{0c}{}^2 \tag{B.6}$$

$$=-\frac{20mD_a}{9\pi a^2}(\mu_e-\mu_h)B_{0c}\left(1+\frac{2sa}{3D_a}\right), \qquad \left|\frac{n_0-p_0}{n_0+p_0}\right|\ll\mu_{e,h}{}^2B_{0c}{}^2. \tag{B.7}$$

As expected, recombination, being a loss mechanism, has raised the threshold fields. However, for the experimental situation of interest: $s\approx 30$ cm/sec, $\tau_b\approx 1400$ $\mu$sec, $a=0.058$ cm, and $D_a\approx 60$ cm$^2$/sec, the correction to $k_c$ and $f_c$ is about 1.5% and that to $B_{0c}$ is about 2.5%. These corrections are less than the experimental error and are therefore negligible.

## APPENDIX C: THRESHOLD CONDITIONS FOR GENERAL AZIMUTHAL MODE

In the dispersion relation (21) we again expand the modified Bessel functions in Taylor series expansions except that now we consider a general $m$ instead of $m=\pm 1$. The case of $m=0$ can be treated and eliminated at the outset. In (21), setting $m=0$ we have simply

$$\alpha\beta kI_0(\beta a)I_0(ka)=0. \tag{C.1}$$

The magnetic field does not enter this expression at all, so there is no threshold. The solutions therefore correspond to damped or evanescent waves and need not be considered further.

For $m\neq 0$ modes we keep only the first two terms of the expansions and substitute them in (21). Proceeding as in Sec. III we arrive at the equivalent of (24) for general $m$:

$$\begin{aligned}k^2a^2[&|m|(|m|+2)+im(|m|+1)(\mu_e-\mu_h)B_0]\\&+i[a^2(\omega-\mu_aE_0k)/2D_a][|m|(|m|+2)\\&+im(|m|+2)\mu_HB_0-im|m|\mu_aB_0]\\&+m\mu_M{}^2E_0B_0ka^2/D_a+2m^2(|m|+1)\\&+2m|m|(|m|+1)(\mu_e-\mu_h)B_0=0.\end{aligned} \tag{C.2}$$

Separating the real and imaginary parts of (C.2) for real $k$ and $\omega$ and eliminating $\omega$ from the resulting pair of equations, we then have

$$|m|(|m|+2)k^2a^2+(m\mu_M{}^2E_0B_0/D_a)ka^2+2(|m|+1)=0. \tag{C.3}$$

Therefore, at threshold

$$k_c{}^2=2|m|(|m|+1)/(|m|+2)a^2 \tag{C.4}$$

and

$$B_{0c}=-\frac{2m(|m|+2)D_ak}{|m|\mu_M{}^2}\frac{1}{E_0}. \tag{C.5}$$

From (C.5) it is evident that the $m=1$ mode has the lowest threshold for growth.

Returning to (C.2) we have, following the derivation of (28) and (29), the threshold frequency:

$$f_c=(1/2\pi)\mu_aE_0k_c, \qquad \left|\frac{n_0-p_0}{n_0+p_0}\right|\gg\mu_{e,h}{}^2B_0{}^2 \tag{C.6}$$

$$=-\frac{2m(|m|+1)(2|m|+1)D_a}{\pi(|m|+2)a^2}(\mu_e-\mu_h)B_{0c}, \qquad \left|\frac{n_0-p_0}{n_0+p_0}\right|\ll\mu_{e,h}{}^2B_0{}^2. \tag{C.7}$$

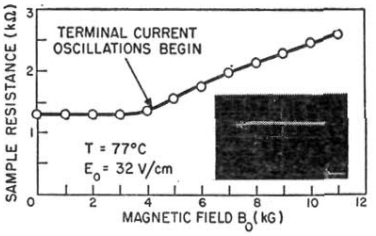


FIG. 15. Average sample resistance versus $B_0$. Inset is oscilloscope trace of terminal current oscillations which begin at the point indicated. Vertical scale: 10 mA/div. Horizontal scale: 200 $\mu$sec/div.

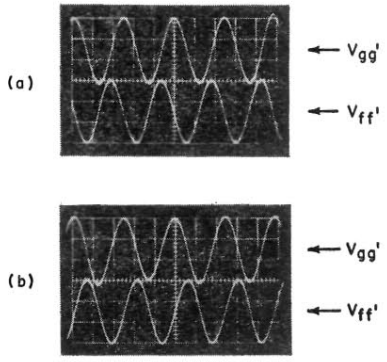


FIG. 4. Oscilloscope traces showing 90° phase difference between signals at probes gg′ and ff′. Set (a) corresponds to $B_0$ parallel to $E_0$ and (b) to $B_0$ antiparallel to $E_0$. Vertical scale: 5 mV/div. Horizontal scale: 10 $\mu$sec/div.